



ASTRO-H Space X-ray Observatory White Paper

White Dwarf

K. Mukai (NASA/GSFC/CRESST & UMBC), T. Yuasa (RIKEN),
A. Harayama (JAXA), T. Hayashi (JAXA), M. Ishida (JAXA), K. S. Long (STScI),
Y. Terada (Saitama University) and M. Tsujimoto (JAXA)
on behalf of the ASTRO-H Science Working Group

Abstract

Interacting binaries in which a white dwarf accretes material from a companion — cataclysmic variables (CVs) in which the mass loss is via Roche-lobe overflow, and symbiotic stars in which the white dwarf captures the wind of a late type giant — are relatively commonplace. They display a wide range of behaviors in the optical, X-rays, and other wavelengths, which still often baffles observers and theorists alike. They are likely to be a significant contributor to the Galactic ridge X-ray emission, and the possibility that some CVs or symbiotic stars may be the progenitors of some of the Type Ia supernovae deserves serious consideration. Furthermore, these binaries serve as excellent laboratories in which to study physics of X-ray emission from high density plasma, accretion physics, reflection, and particle acceleration. *ASTRO-H* is well-matched to the study of X-ray emission from many of these objects. In particular, the excellent spectral resolution of the SXS will enable dynamical studies of the X-ray emitting plasma. We also discuss the possibility of identifying an accreting, near-Chandrasekhar-mass white dwarf by measuring the gravitational redshift of the 6.4 keV line.

Complete list of the ASTRO-H Science Working Group

Tadayuki Takahashi^a, Kazuhisa Mitsuda^a, Richard Kelley^b, Felix Aharonian^c, Hiroki Akamatsu^d, Fumie Akimoto^e, Steve Allen^f, Naohisa Anabuki^g, Lorella Angelini^b, Keith Arnaud^b, Marc Audardⁱ, Hisamitsu Awaki^j, Aya Bamba^k, Marshall Bautz^l, Roger Blandford^f, Laura Brenneman^b, Greg Brown^m, Edward Cackettⁿ, Maria Chernyakova^c, Meng Chiao^b, Paolo Coppi^o, Elisa Costantini^d, Jelle de Plaa^d, Jan-Willem den Herder^d, Chris Done^p, Tadayasu Dotani^a, Ken Ebisawa^a, Megan Eckart^b, Teruaki Enoto^q, Yuichiro Ezoe^r, Andrew Fabianⁿ, Carlo Ferrignoⁱ, Adam Foster^s, Ryuichi Fujimoto^l, Yasushi Fukazawa^u, Stefan Funk^f, Akihiro Furuzawa^e, Massimiliano Galeazzi^v, Luigi Gallo^w, Poshak Gandhi^p, Matteo Guainazzi^x, Yoshito Haba^y, Kenji Hamaguchi^h, Isamu Hatsukade^z, Takayuki Hayashi^a, Katsuhiro Hayashi^a, Kiyoshi Hayashida^g, Junko Hiraga^{aa}, Ann Hornschemeier^b, Akio Hoshino^{ab}, John Hughes^{ac}, Una Hwang^{ad}, Ryo Iizuka^a, Yoshiyuki Inoue^a, Hajime Inoue^a, Kazunori Ishibashi^e, Manabu Ishida^a, Kumi Ishikawa^q, Yoshitaka Ishisaki^f, Masayuki Ito^{ae}, Naoko Iyomoto^{af}, Jelle Kaastra^d, Timothy Kallman^b, Tuneyoshi Kamae^f, Jun Kataoka^{ag}, Satoru Katsuda^a, Junichiro Katsuta^u, Madoka Kawaharada^a, Nobuyuki Kawai^{ah}, Dmitry Khangulyan^a, Caroline Kilbourne^b, Masashi Kimura^{ai}, Shunji Kitamoto^{ab}, Tetsu Kitayama^{aj}, Takayoshi Kohmura^{ak}, Motohide Kokubun^a, Saori Konami^r, Katsuji Koyama^{al}, Hans Krimm^b, Aya Kubota^{am}, Hideyo Kunieda^e, Stephanie LaMassa^o, Philippe Laurent^{an}, François Lebrun^{an}, Maurice Leutenegger^b, Olivier Limousin^{an}, Michael Loewenstein^b, Knox Long^{ao}, David Lumb^{ap}, Grzegorz Madejski^f, Yoshitomo Maeda^a, Kazuo Makishima^{aa}, Maxim Markevitch^b, Hironori Matsumoto^e, Kyoko Matsushita^{aq}, Dan McCammon^{ar}, Brian McNamara^{as}, Jon Miller^{at}, Eric Miller^l, Shin Mineshige^{au}, Ikuyuki Mitsuishi^e, Takuya Miyazawa^e, Tsunefumi Mizuno^u, Koji Mori^z, Hideyuki Mori^e, Koji Mukai^b, Hiroshi Murakami^{av}, Toshio Murakami^t, Richard Mushotzky^h, Ryo Nagino^g, Takao Nakagawa^a, Hiroshi Nakajima^g, Takeshi Nakamori^{aw}, Shinya Nakashima^a, Kazuhiro Nakazawa^{aa}, Masayoshi Nobukawa^{al}, Hirofumi Noda^q, Masaharu Nomachi^{ax}, Steve O' Dell^{ay}, Hirokazu Odaka^a, Takaya Ohashi^r, Masanori Ohno^u, Takashi Okajima^b, Naomi Ota^{az}, Masanobu Ozaki^a, Frits Paerels^{ba}, Stéphane Paltaniⁱ, Arvind Parmar^x, Robert Petre^b, Ciro Pintoⁿ, Martin Pohlⁱ, F. Scott Porter^b, Katja Pottschmidt^b, Brian Ramsey^{ay}, Rubens Reis^{at}, Christopher Reynolds^h, Claudio Ricci^{au}, Helen Russellⁿ, Samar Safi-Harb^{bb}, Shinya Saito^a, Hiroaki Sameshima^a, Goro Sato^{ag}, Kosuke Sato^{aq}, Rie Sato^a, Makoto Sawada^k, Peter Serlemitsos^b, Hiromi Seta^{bc}, Aurora Simionescu^a, Randall Smith^s, Yang Soong^b, Łukasz Stawarz^a, Yasuharu Sugawara^{bd}, Satoshi Sugita^j, Andrew Szymkowiak^o, Hiroyasu Tajima^e, Hiromitsu Takahashi^u, Hiroaki Takahashi^g, Yoh Takei^a, Toru Tamagawa^q, Takayuki Tamura^a, Keisuke Tamura^e, Takaaki Tanaka^{al}, Yasuo Tanaka^a, Yasuyuki Tanaka^u, Makoto Tashiro^{bc}, Yuzuru Tawara^e, Yukikatsu Terada^{bc}, Yuichi Terashima^j, Francesco Tombesi^b, Hiroshi Tomida^{ai}, Yohko Tsuboi^{bd}, Masahiro Tsujimoto^a, Hiroshi Tsunemi^g, Takeshi Tsuru^{al}, Hiroyuki Uchida^{al}, Yasunobu Uchiyama^{ab}, Hideki Uchiyama^{be}, Yoshihiro Ueda^{au}, Shutaro Ueda^g, Shiro Ueno^{ai}, Shinichiro Uno^{bf}, Meg Urry^o, Eugenio Ursino^v, Cor de Vries^d, Shin Watanabe^a, Norbert Werner^f, Dan Wilkins^w, Shinya Yamada^r, Hiroya Yamaguchi^b, Kazutaka Yamaoka^e, Noriko Yamasaki^a, Makoto Yamauchi^z, Shigeo Yamauchi^{az}, Tahir Yaqoob^b, Yoichi Yatsu^{ah}, Daisuke Yonetoku^t, Atsumasa Yoshida^k, Takayuki Yuasa^q, Irina Zhuravleva^f, Abderahmen Zoghbi^h, and John ZuHone^b

^aInstitute of Space and Astronautical Science (ISAS), Japan Aerospace Exploration Agency (JAXA), Kanagawa 252-5210, Japan

^bNASA/Goddard Space Flight Center, MD 20771, USA

^cAstronomy and Astrophysics Section, Dublin Institute for Advanced Studies, Dublin 2, Ireland

^dSRON Netherlands Institute for Space Research, Utrecht, The Netherlands

^eDepartment of Physics, Nagoya University, Aichi 338-8570, Japan

^fKavli Institute for Particle Astrophysics and Cosmology, Stanford University, CA 94305, USA

^gDepartment of Earth and Space Science, Osaka University, Osaka 560-0043, Japan

^hDepartment of Astronomy, University of Maryland, MD 20742, USA

ⁱUniversité de Genève, Genève 4, Switzerland

^jDepartment of Physics, Ehime University, Ehime 790-8577, Japan

^kDepartment of Physics and Mathematics, Aoyama Gakuin University, Kanagawa 229-8558, Japan

^lKavli Institute for Astrophysics and Space Research, Massachusetts Institute of Technology, MA 02139, USA

^mLawrence Livermore National Laboratory, CA 94550, USA

ⁿInstitute of Astronomy, Cambridge University, CB3 0HA, UK

^oYale Center for Astronomy and Astrophysics, Yale University, CT 06520-8121, USA

^pDepartment of Physics, University of Durham, DH1 3LE, UK

^qRIKEN, Saitama 351-0198, Japan

^rDepartment of Physics, Tokyo Metropolitan University, Tokyo 192-0397, Japan

^sHarvard-Smithsonian Center for Astrophysics, MA 02138, USA

- ^tFaculty of Mathematics and Physics, Kanazawa University, Ishikawa 920-1192, Japan
- ^uDepartment of Physical Science, Hiroshima University, Hiroshima 739-8526, Japan
- ^vPhysics Department, University of Miami, FL 33124, USA
- ^wDepartment of Astronomy and Physics, Saint Mary's University, Nova Scotia B3H 3C3, Canada
- ^xEuropean Space Agency (ESA), European Space Astronomy Centre (ESAC), Madrid, Spain
- ^yDepartment of Physics and Astronomy, Aichi University of Education, Aichi 448-8543, Japan
- ^zDepartment of Applied Physics, University of Miyazaki, Miyazaki 889-2192, Japan
- ^{aa}Department of Physics, University of Tokyo, Tokyo 113-0033, Japan
- ^{ab}Department of Physics, Rikkyo University, Tokyo 171-8501, Japan
- ^{ac}Department of Physics and Astronomy, Rutgers University, NJ 08854-8019, USA
- ^{ad}Department of Physics and Astronomy, Johns Hopkins University, MD 21218, USA
- ^{ae}Faculty of Human Development, Kobe University, Hyogo 657-8501, Japan
- ^{af}Kyushu University, Fukuoka 819-0395, Japan
- ^{ag}Research Institute for Science and Engineering, Waseda University, Tokyo 169-8555, Japan
- ^{ah}Department of Physics, Tokyo Institute of Technology, Tokyo 152-8551, Japan
- ^{ai}Tsukuba Space Center (TKSC), Japan Aerospace Exploration Agency (JAXA), Ibaraki 305-8505, Japan
- ^{aj}Department of Physics, Toho University, Chiba 274-8510, Japan
- ^{ak}Department of Physics, Tokyo University of Science, Chiba 278-8510, Japan
- ^{al}Department of Physics, Kyoto University, Kyoto 606-8502, Japan
- ^{am}Department of Electronic Information Systems, Shibaura Institute of Technology, Saitama 337-8570, Japan
- ^{an}IRFU/Service d'Astrophysique, CEA Saclay, 91191 Gif-sur-Yvette Cedex, France
- ^{ao}Space Telescope Science Institute, MD 21218, USA
- ^{ap}European Space Agency (ESA), European Space Research and Technology Centre (ESTEC), 2200 AG Noordwijk, The Netherlands
- ^{aq}Department of Physics, Tokyo University of Science, Tokyo 162-8601, Japan
- ^{ar}Department of Physics, University of Wisconsin, WI 53706, USA
- ^{as}University of Waterloo, Ontario N2L 3G1, Canada
- ^{at}Department of Astronomy, University of Michigan, MI 48109, USA
- ^{au}Department of Astronomy, Kyoto University, Kyoto 606-8502, Japan
- ^{av}Department of Information Science, Faculty of Liberal Arts, Tohoku Gakuin University, Miyagi 981-3193, Japan
- ^{aw}Department of Physics, Faculty of Science, Yamagata University, Yamagata 990-8560, Japan
- ^{ax}Laboratory of Nuclear Studies, Osaka University, Osaka 560-0043, Japan
- ^{ay}NASA/Marshall Space Flight Center, AL 35812, USA
- ^{az}Department of Physics, Faculty of Science, Nara Women's University, Nara 630-8506, Japan
- ^{ba}Department of Astronomy, Columbia University, NY 10027, USA
- ^{bb}Department of Physics and Astronomy, University of Manitoba, MB R3T 2N2, Canada
- ^{bc}Department of Physics, Saitama University, Saitama 338-8570, Japan
- ^{bd}Department of Physics, Chuo University, Tokyo 112-8551, Japan
- ^{be}Science Education, Faculty of Education, Shizuoka University, Shizuoka 422-8529, Japan
- ^{bf}Faculty of Social and Information Sciences, Nihon Fukushi University, Aichi 475-0012, Japan

Contents

1	Top Science	5
2	Introduction	5
2.1	Abbreviations	6
3	Gravitationally redshifted 6.4 keV line in massive accreting WDs	6
3.1	Background and Previous Studies	6
3.2	Prospects & Strategy	6
3.3	Targets & Feasibility	7
3.4	Beyond Feasibility	8
4	Detailed structure of the post-shock region in magnetic CVs	9
4.1	Background and Previous Studies	9
4.2	Prospects & Strategy	10
4.2.1	Density diagnostics with Fe XXV triplets	10
4.2.2	Spectral model of the PSR updated for the SXS observation	10
4.3	Targets & Feasibility	11
4.3.1	V1223 Sgr, the brightest magnetic CV, as an appropriate target	11
4.3.2	Simulation of SXS spectra	12
4.4	Beyond Feasibility	13
5	Refecation in accreting WDs	14
5.1	Background and Previous Studies	14
5.2	Prospects & Strategy	14
5.3	Targets & Feasibility	14
5.4	Beyond Feasibility	15
6	X-ray emission region in non-magnetic CVs	15
6.1	Background and Previous Studies	15
6.2	Prospects & Strategy	16
6.3	Targets & Feasibility	17
7	Anisotropic Radiative Transfer of Resonance photons	18
7.1	Background and Previous Studies	18
7.2	Prospects & Strategy	21
7.3	Targets & Feasibility	21

1 Top Science

The highest priority science of *ASTRO-H* for white dwarfs is the search for extremely massive white dwarfs with high accretion rates. We propose to do so by measuring the gravitational redshift of the 6.4 keV fluorescent Fe line from the white dwarf surface using the SXS.

Observationally speaking, this is a relatively simple experiment, as long as a precise and accurate gain calibration is available for the SXS. There are potential targets which are known to have a strong enough 6.4 keV line and is thought to harbor a near Chandrasekhar mass white dwarf. Unlike some other worthy investigations regarding accreting white dwarfs, this is a study that requires X-ray spectroscopy, while requiring relatively little multiwavelength support. Finally, if we can determine just one white dwarf mass above $1.3 M_{\odot}$ sufficient accurately, that would be a major result with implications on the debate over Type Ia supernova progenitor channels.

2 Introduction

Some white dwarfs in CVs (and possibly also symbiotic stars) are magnetic enough that accretion proceeds along field lines. The accretion flow in such cases is nearly vertical with respect to the white dwarf surface. A strong stand-off shock forms just above the white dwarf surface; the post-shock plasma must cool and further slow down before settling onto the white dwarf. This cooling often happens primarily via emission of optically thin, thermal X-rays. For a $0.6 M_{\odot}$ white dwarf, the free-fall velocity is $\sim 4,300 \text{ km s}^{-1}$ and the shock temperature is $\sim 22 \text{ keV}$ ($6,900 \text{ km s}^{-1}$ and 57 keV for a $1.0 M_{\odot}$ white dwarf). For a specific accretion rate of $1 \text{ g s}^{-1} \text{ cm}^{-2}$, the immediate post-shock density is $\sim 10^{15} \text{ cm}^{-3}$ ($\sim 6 \times 10^{15} \text{ cm}^{-3}$), the post-shock cooling timescale is 0.7 s (1.8 s), and the shock height is 5% of the white dwarf radius, or $0.05 R_{\text{WD}}$ ($0.34 R_{\text{WD}}$). This basic picture of the accretion column has been known for 40 years (Aizu, 1973). The observed X-ray emission should be the sum of emission at many temperatures, as the plasma cools, slows down, and becomes denser. We explore below whether we can obtain direct quantitative observational confirmation of this picture using velocity and density diagnostics of the high spectral resolution SXS data.

In non-magnetic CVs, the accretion proceeds via a disk. This is probably also true of the majority of symbiotic stars that have been detected above $\sim 2 \text{ keV}$ to date. In such cases, the X-rays are emitted from the boundary layer between the Keplerian disk and the white dwarf surface; the physics of the boundary layer is far more complex than that of the accretion column. Can we apply similar diagnostics as for magnetic CVs to aide the theoretical efforts to understand the boundary layer? Moreover, while our understanding of the steady-state accretion disk is fairly secure, it is less so for dwarf novae, for which the disk instability model (DIM) is widely adopted as the explanation. However, the basic version of DIM predicts the matter transferred from the secondary to pile up in the disk during quiescence (the low state) and hence very little accretion to take place onto the white dwarf. The observed X-ray luminosity is much higher than predicted. One possible modification of the DIM is that the quiescent disk has a central hole, replaced by an advective flow. We will explore if *ASTRO-H* can constrain the reflection amplitude with sufficient accuracy to determine if such a hole exists in the quiescent disk.

If we can identify even a single massive white dwarf, close to the Chandrasekhar limit, in an accreting binary, such a discovery have a profound implications. The presence of such a binary is an important precondition for the single degenerate channel of Type Ia supernovae. Conventional methods such as optical radial velocity studies have not led to a secure identification of such a system. We believe that the *ASTRO-H* SXS can measure the gravitational redshift of the 6.4 keV line produced via reflection on the white dwarf surface, if it is sufficiently massive. Although success is not guaranteed, we consider this to be the most important *ASTRO-H* science topic for accreting white dwarf binaries.

The 2–10 keV luminosity of CVs and symbiotic stars range from $\sim 10^{29} \text{ ergs s}^{-1}$ for the low accretion rate dwarf novae (Reis et al., 2013) to $> 10^{34} \text{ ergs s}^{-1}$ for the *Swift* BAT detected symbiotic stars (Kennea et al., 2009). Given their relative proximity (of order 100 pc for many CVs and of order 2 kpc for numerous symbiotic stars), the potential target list numbers several dozen.

2.1 Abbreviations

BL Boundary Layer via which gas from an accretion disk settles on to the white dwarf surface

CV Cataclysmic Variable containing mass-accreting white dwarf

DIM Disk Instability Model

PSR Post-Shock Region of an accretion column

TNR Thermo-Nuclear Runaway

WD White Dwarf star

3 Gravitationally redshifted 6.4 keV line in massive accreting WDs

3.1 Background and Previous Studies

For the single degenerate channel for Type Ia supernovae to be viable, there must exist accreting binaries hosting massive (near Chandrasekhar mass) WDs. The WD mass in CVs and symbiotic stars would show a secular increase if accretion was the only factor involved. However, under many conditions, accreting WDs undergo thermonuclear runaways (TNRs) whenever a sufficient mass is accumulated. Such events are observed as nova eruptions, in which a large amount of mass is ejected from the WD surface. Observations often show the nova ejecta to be enriched by the underlying WD material. Given this, it is unclear if WDs can grow in mass through successive accretion-TNR cycles, and if so, under what conditions and at what efficiency (fraction of the accreted mass that is retained by the WD). This is a significant weakness of the single degenerate channel.

Given this, even a discovery of single system with, say, $> 1.3 M_{\odot}$ WD would be significant. Such a binary was likely born with a somewhat less massive WD, with the WD mass growing over time; if the WD mass is decreasing, the initial mass of the WD must be even closer to the Chandrasekhar limit, which seems an unlikely possibility. Such a discovery would prove that one of the necessary conditions for the single degenerate channel to be viable is met.

There are indirect indications for high WD masses in accreting binaries. For example, recurrent novae — accreting WDs that have been seen to experience nova eruptions multiple times over the last century or so — are likely to have high mass WDs. This is because the critical density required for a TNR is unlikely to be reached within a span of a few decades after the previous TNR, unless the gravitational field of the WD is exceptionally strong. However, this line of reasoning is qualitative and not foolproof.

Direct observational determinations of WD mass in accreting binaries are often very imprecise. Dynamical determination relies on radial velocity studies, but few accreting WD systems are double-line spectroscopic binaries — the mass donors in CVs are often too faint, and those in symbiotic stars are too bright. Also, the radial velocity motion of the WD is usually inferred via the motion of accretion disk around it; any asymmetries or azimuthal structures can easily mislead us. Furthermore, the binary inclination is uncertain unless the system is eclipsing, which often translates to large uncertainties in the derived WD mass.

If we can measure the gravitational redshift of spectral features from the white dwarf surface, this can all change. We believe there is a strong possibility that we can do so, by using *ASTRO-H* SXS to measure the energy of the 6.4 keV line precisely.

3.2 Prospects & Strategy

For this method to work, several conditions must be met. The target must be hard X-ray bright, with a significant 6.4 keV line as seen in previous observations. A large fraction of the 6.4 keV line flux must originate on the WD surface. The systemic velocity of the binary must be known, and ideally the orbital motion of the WD negligible ($\sim 10 \text{ km s}^{-1}$). Most importantly, the WD must be sufficiently massive that the gravitational redshift can be measured against statistical and systematic uncertainties.

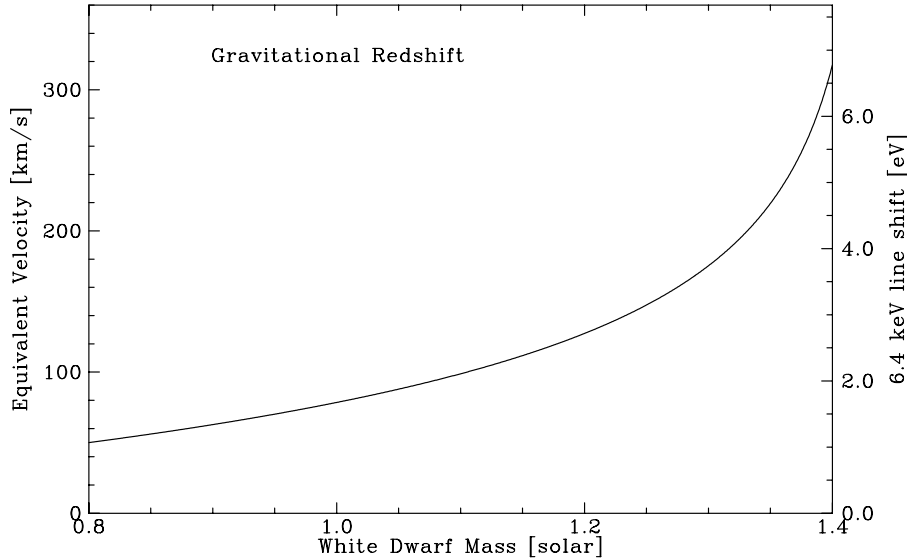


Figure 1: Gravitational redshift as a function of the WD mass, expressed in equivalent velocity and as energy shift for the 6.4 keV line.

We show the expected degree of gravitational redshift in Figure 1. As can be seen, the more massive the WD, the easier it will be to detect the redshift. For WD mass above $1.1 M_{\odot}$, the redshift will be larger than 2 eV, which we argue is easily within reach of SXS measurements. Moreover, the gravitational redshift is a sensitive proxy of the WD mass just below the Chandrasekhar limit, precisely where a mass determination can have a significant impact.

The first criterion can be satisfied by selecting a target detected in the *Swift* BAT survey of the hard X-ray sky. Several dozen accreting WD systems have been detected to date, but most are magnetic CVs with only moderately massive WDs ($0.8 - 1.0 M_{\odot}$). Here we concentrate on the 4 symbiotic stars detected in the BAT survey (Kennea et al., 2009). Since the M giant mass donor is the dominant source of optical and IR photons, their systemic velocity is (or can be) known accurately. Due to the large orbit and the long orbital period, the radial velocity motion of the WD is relatively small. Finally, there is no evidence that the WDs in these symbiotic stars are magnetic. Therefore, the very fact that they are detected by BAT indicates that the WDs are massive (note that, for a given WD mass, the maximum temperature of the shock is factor of ~ 2 higher in the magnetic than in the non-magnetic case, due to the difference in free-fall and Keplerian velocities).

3.3 Targets & Feasibility

One of the 4 symbiotic stars detected by BAT is T CrB, which is also a recurrent nova. Both this fact and the hard BAT spectrum indicates that its WD is exceptionally massive, perhaps around $1.35 M_{\odot}$. It has been always active and hard X-ray bright during the BAT survey. The WD photosphere is hidden in the optical/UV by the bright emissions from the M giant mass donor and the accretion disk. T CrB exhibits a strong 6.4 keV line, partly from the reflection off the WD surface. We therefore believe that T CrB is the best target for this study.

We guide our simulation (Figure 2) using the 46 ks *Suzaku* observation obtained in 2006. The XIS data are fit using a mildly broadened *mkcflow* model absorbed by a partial covering absorber with a single, narrow Gaussian at 6.396 keV. The inset shows the difference between this simulation and one with a narrow Gaussian at 6.400 keV. This clearly shows that the *ASTRO-H* SXS has the statistical quality necessary to detect a gravitational redshift of 4 eV. In the simulation, the following SXS instrumental response files were used:

- `ah_sxs_5ev_basefilt_20100712.rmf` (energy redistribution file),
- `sxt-s_120210_ts02um_intallpxl.arf` (auxiliary response file), and

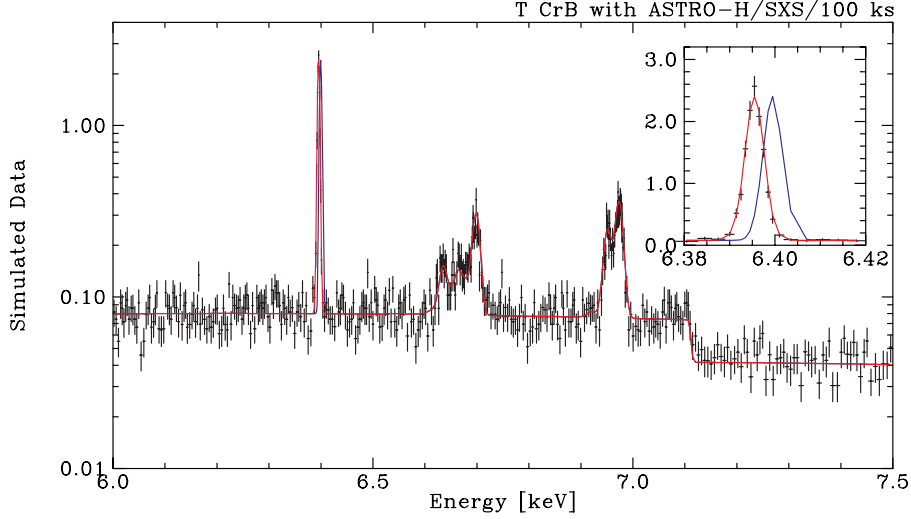


Figure 2: Simulated *ASTRO-H* SXS 100 ks observation of T CrB in the Fe $K\alpha$ region.

- `sxs_cxb+nx_b_5eV_20110211_1Gs.pha` (background spectral file).

We need to consider two further factors. One is the accuracy of gain calibration. On this point, we propose to observe T CrB with the calibration source on to obtain the best possible gain calibration. With this, it is likely that the gain calibration is accurate enough for our purpose. However, we will pay close attention to this issue during ground calibration and revisit our observing plan if necessary.

Another complication is that the intrinsic energy of the fluorescent line is not fixed at 6.400 keV, and is in fact a function of the ionization state of Fe. The ionization state of Fe in the relevant layer of the WD atmosphere is unknown. Reflection requires high column density of order 10^{24} cm^{-2} , i.e., at or near the WD photosphere. If the white dwarf is hot, that alone (without irradiation from above) can ionize Fe in the photosphere. For example, lines of Fe VII and Fe VIII are often seen in the photospheric spectra of PG 1159 type stars (hot, hydrogen deficient post-AGB stars), and up to Fe X in the hottest cases such as PG 1159–035 ($T_{\text{eff}}=140,000\text{K}$, $\log g=7$; Werner et al. 2011). Since the photospheric densities are high (of order $3 \times 10^{-5} \text{ g cm}^{-3}$), and the hard X-ray luminosity is modest ($\sim 10^{34} \text{ ergs s}^{-1}$), photoionization is unlikely to result in ionization states higher than these. Nevertheless, the Fe $K\alpha$ energies change from 6.4055/6.3917 keV for Fe II to 6.4029/6.3900 keV for Fe VIII (Palmeri et al., 2003). However, the Fe $K\beta$ line energy changes much more significantly, and in the opposite direction: 7.0583 keV for Fe II and 7.0740 keV for Fe VIII. Thus, we will design our observation to be able to detect the Fe $K\beta$ line, roughly 15% the flux of the Fe $K\alpha$ line. If we can detect both, the ionization state of Fe and the gravitational redshift can both be determined from SXS data.

3.4 Beyond Feasibility

In addition, we can measure the maximum temperature in the shock, kT_{max} using the HXI data. In a 100 ks observation, we estimate a statistical accuracy of about $\pm 2 \text{ keV}$. Actual accuracy depends on the parameter degeneracy between kT_{max} and the reflection amplitude, background subtraction accuracy and other systematics. This will provide a good cross-check for the gravitational redshift measurement.

The spectrum of T CrB is highly absorbed, and the nature of intrinsic absorber in symbiotic stars is poorly understood. The proposed observation will provide the most precise determination yet of the absorber, including any variability during the observation.

Finally, we will also obtain high quality spectra of the He-like and H-like lines of Fe. We will extract dynamical information regarding the post-shock region from these lines, as we propose to do for SS Cyg. If the emission region is sufficiently close to the white dwarf, the H-like lines will also be gravitationally redshifted.

If that is the case, it is in some way a cleaner measurement than the reflection line, since the ionization state of the line-producing ions is not in doubt in this case.

4 Detailed structure of the post-shock region in magnetic CVs

4.1 Background and Previous Studies

As mentioned previously, the basic picture of the post-shock region (PSR) of magnetic CVs is relatively secure. However, the specific accretion rate (or, conversely, the fractional area of the white dwarf surface onto which accretion occurs) is a key parameter that is poorly known. It is determined by the complex interaction between the accretion flow and the magnetic field, which is difficult to solve purely theoretically. In practice, we can treat the specific accretion rate (usually assumed to be uniform across the accretion column) as a free parameter, then solve for the temperature, velocity, and density structure of the PSR, and then predict the resulting multi-temperature X-ray spectrum. We can then fit such models to the observed X-ray spectrum to obtain, e.g., the white dwarf mass (Yuasa et al., 2010). Figures 3 and 4 present a schematic view of a PSR, and post-shock plasma density/temperature profiles obtained by solving numerical hydrostatic equations shown in Yuasa et al. (2010). In the figures, typical parameters are set assuming those of V1223 Sagittarii, one of the classical magnetic CVs that has relatively high accretion rate.

For most magnetic CVs, the PSR density is expected to be so high that He-like triplets that can be resolved with *Chandra* HETG do not help. In addition, the HETG has a small effective area, so it is not practical for most magnetic CVs. The only exception is a highly atypical magnetic CV, EX Hya, for which some density information has been obtained using Fe L density diagnostics (Mauche et al., 2003).

The *ASTRO-H* SXS will be able to resolve Fe XXV triplets into separate lines providing considerably larger effective area at the same time. Because of this, we aim to perform density diagnostics based on Fe XXV triplets and constrain the geometry of a PSR for selected magnetic CVs. Determination of the geometry will lead to precise calculation of density, temperature, and velocity distribution along the PSR, and further understanding on accretion physics and magnetic field structure of CVs.

For review of density and temperature diagnostic methods using triplets from He-like ions, see Porquet et al. (2010).

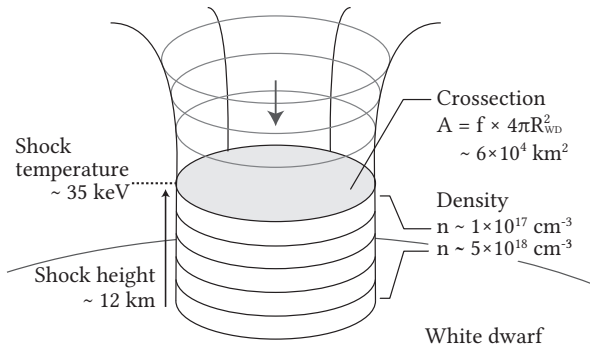


Figure 3: Schematic view of an accretion column and a post-shock region of an intermediate polar). Values presented in the figure are calculated using typical accretion condition of V1223 Sgr; $M_{WD} = 0.79 M_{\odot}$, $f = 0.001$ and $dM/dt = 8.4 \times 10^{16} \text{ g s}^{-1}$ (Yuasa et al., 2010; Hayashi et al., 2011).

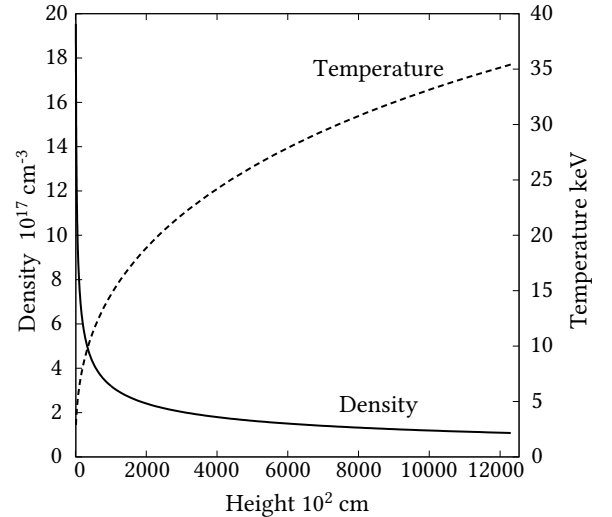


Figure 4: Plasma density and plasma temperature profiles in the post-shock region calculated using the numerical hydrostatic model of Yuasa et al. (2010). Assumed accretion parameters are the same as presented in Figure 3.

4.2 Prospects & Strategy

4.2.1 Density diagnostics with Fe XXV triplets

Figure 5 shows radiative transitions of Fe XXV ions. The intensity of the forbidden line ($^3S_1 - ^1S_0$) is strongly dependent on the plasma density. Above a “critical density” collisional de-excitation from 3S_1 to 1S_0 becomes the dominant process and the “forbidden” radiative decay is suppressed. The forbidden-intercombination line intensity ratio $R \equiv z/(x + y)$, where x , y and z are intensities of corresponding lines, can therefore be used to measure the density of originating plasma based on observed spectra. Figure 6 illustrates this dependence based on triplet line intensities calculated with the collisional ionization equilibrium (CIE) model available in the SPEX analysis package (Kaastra et al., 1996). Based on this curve, the critical density of Fe XXV triplet is $\sim 10^{17} - 10^{18} \text{ cm}^{-3}$.

Astrophysical plasmas with a density above the critical density of Fe XXV together with plasma temperature that is high enough to ionize Fe to He-like are rather rare. However, PSRs of magnetic CVs with high accretion rates are believed to reach this extreme condition as exemplified in Figures 3 and 4. Therefore, by studying the Fe XXV triplet lines with the SXS, plasma density in a PSR could be directly measured, and it will be possible to constrain the physical condition of a PSR further deepening our understanding on accretion physics.

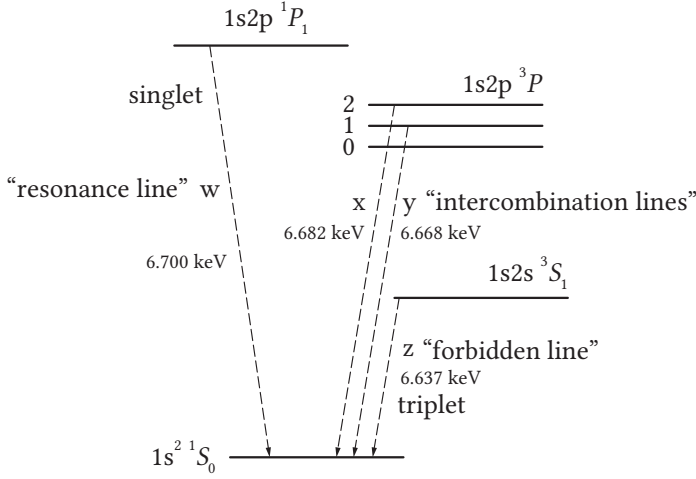


Figure 5: Radiative transitions of Fe XXV ions relevant to the present magnetic CV studies. See Gabriel & Jordan (1969); Porquet et al. (2010) for details.

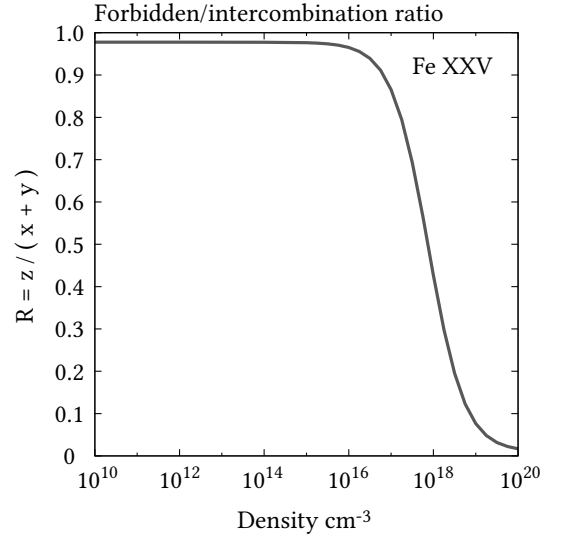


Figure 6: He-like $R = z/(x + y) = f/i$ line ratio of Fe.

4.2.2 Spectral model of the PSR updated for the SXS observation

To evaluate feasibility of the density diagnostics based on the Fe XXV triplet line ratio, we updated the X-ray spectral model of the PSR (Yuasa et al., 2010), using the CIE model of the SPEX replacing the APEC CIE model. Essence of this model construction is to convolve the emission measure distribution and single temperature CIE spectrum over the whole PSR. By doing so, the new model is now able to include the density dependence of the forbidden/intercombination lines correctly accounting the multi-temperature nature of the PSR plasma.

When calculating the spectral model, it is necessary to fix (or provide) a WD mass value which is the primary free parameter that changes model spectral shape, and the geometrical area of the PSR as the fraction of the WD surface area. This is because, for a fixed total accretion rate, the density of a PSR depends on the area over which accretion occurs, and so do solutions of the hydrostatic equations used in the model (i.e. different density/temperature distributions can be obtained). In the present paper, we use f parameter, which is defined as a ratio of accretion column cross section to the WD surface area, to denote the geometrical size of the PSR.

Three example values, 0.0002, 0.001, and 0.005 are chosen from a possible range of this parameter based on previous studies of magnetic CVs (e.g. Hellier 1997).

As illustrated in Figure 7, the hydrostatic equations of a PSR with different values of f result in different PSR structures, especially in terms of shock heights and plasma density below the shock. Qualitatively, this can be understood that as the PSR cross section gets smaller, the plasma density should increase leading to effective plasma cooling. With high densities, shock heated plasma can cool down effectively, and satisfy the “zero temperature” boundary condition at the bottom of the PSR even if it has higher shock temperature (i.e. smaller shock height) compared to PSRs with larger f values.

After fixing f at the values listed above, we calculated total spectra emitted from assumed PSRs as presented in Figure 4. To apply the spectral model to SXS observation simulation in the following sections, we used the estimated parameters of V1223 Sgr in the calculation as listed in Table 1. Table 2 presents calculation results of some representative values. Note that, in the calculation, we also took into account redshift caused by the bulk motion, or falling velocity, of plasma which amounts about 1500 km s^{-1} at the top of a PSR although the redshift is little apparent in the resulting spectra (this is because most of Fe XXV $K\alpha$ emission comes from regions where falling velocity is small, i.e. lower parts of a PSR).

It is apparent from Figure 6 that the forbidden line (labeled z) is sensitive to f , i.e., as f decreases (or plasma density below the shock increases) intensity of the line decreases due to depopulation of 3S_1 level by collisional excitation (see above). This confirms our previous prospect that the R ratio can be used for density diagnostics of PSRs of magnetic CVs with high accretion rates like V1223 Sgr.

Table 1: Parameter values assumed in the PSR structure model calculation.

Assumed values		Note
M_{WD}	$0.79 M_{\odot}$	WD mass (Yuasa, 2013).
R_{WD}	7070 km	WD radius calculated for $0.79 M_{\odot}$ WD using (Nauenberg, 1972).
dM/dt	$8.4 \times 10^{16} \text{ g s}^{-1}$	Total mass accretion rate (Hayashi et al., 2011).
Z	$0.29 Z_{\odot}$	Metal abundance of accreting gas.

Table 2: Result of the PSR structure model calculation.

Result	f		
	0.0002	0.001	0.005
$h_s \text{ cm}$	2.52×10^5	1.25×10^6	6.14×10^6
$kT_s \text{ keV}$	35.7	35.7	35.4
$\rho_s \text{ cm}^{-3}$	5.42×10^{17}	1.08×10^{17}	2.18×10^{16}
$v_s \text{ cm s}^{-1}$	1.36×10^8	1.36×10^8	1.36×10^8

* h_s , kT_s , ρ_s , and v_s are shock height measured from the WD surface, plasma temperature, density, and falling velocity directly below the shock.

4.3 Targets & Feasibility

4.3.1 V1223 Sgr, the brightest magnetic CV, as an appropriate target

To perform precise density diagnostics, it is essential to select targets that have enough high X-ray flux for high counting statistics and accretion rates that result PSR density higher than the critical density of Fe XXV triplet lines. For selecting appropriate target based on the present knowledge, we created histograms of 2 – 10 keV flux and mass accretion rate as shown in Figure 9. As can be easily seen in the histograms, V1223 Sgr is one of

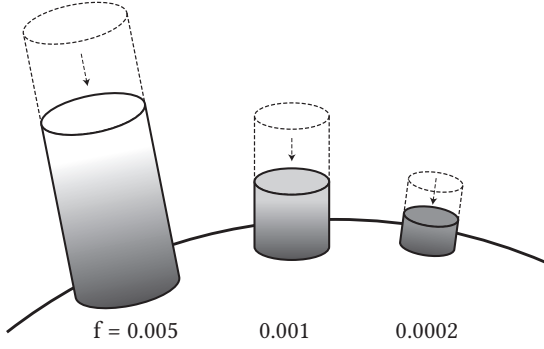


Figure 7: Schematic view of PSR structures with different cross sections but the same total mass accretion rates. The thicker parts correspond to higher densities. The scale of the PSR and the shock heights are exaggerated.

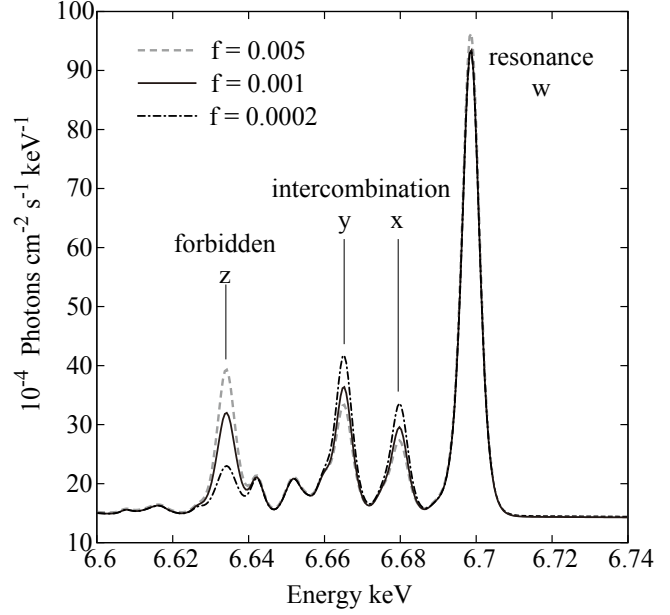


Figure 8: Close-up view of Fe XXV $K\alpha$ spectra of X-ray emission calculated for multi-temperature and multi-density post-shock plasma of V1223 Sgr. Dashed, solid, and dash-dotted curves are calculated with three different covering fraction f of 0.005, 0.001, and 0.0002. Note that the solid curve corresponds to total spectrum expected from temperature/density the distribution presented in Figure 4.

the brightest well known magnetic CVs, and at the same time, it has a relatively high total mass accretion that can create different forbidden line intensities depending on the PSR cross section f (as presented in Figure 8).

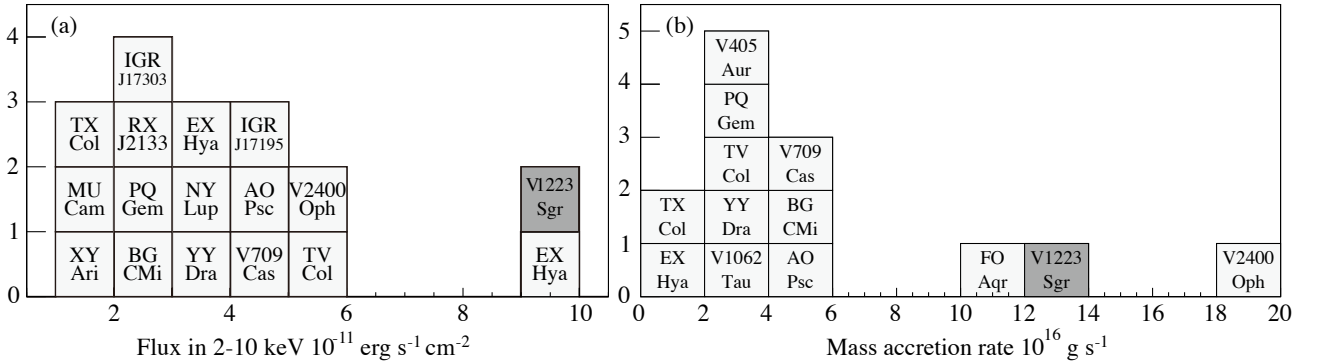


Figure 9: Histograms of (a) 2 – 10 keV flux and (b) mass accretion rate of well-studied classical magnetic CVs (intermediate polars). To highlight V1223 Sgr, bins with an entry for the source is labeled with source name. Data from Yuasa et al. (2010) and Suleimanov et al. (2005).

Based on these facts, V1223 Sgr is an ideal target for an early observation with *ASTRO-H*. Not only the density diagnostics, but studies of X-ray reflection at the WD surface can be performed at the same time using a single observation of V1223 Sgr (see next section).

4.3.2 Simulation of SXS spectra

Using the calculated spectral model (Figure 4), we simulated spectra obtained with the SXS using the following instrumental response files:

- `ah_sxs_5ev_basefilt_20100712.rmf` (energy redistribution file),
- `sxt-s_100208_ts02um_intallpxl.arf` (auxiliary response file), and
- `sxs_nxb_5ev_20110211_1Gs.pha` (background spectral file).

We assumed a net exposure of 100 ks to achieve statistically sufficient photon counts for detailed analysis of w, x, y, and z line intensities. Figure 8 presents three resulting spectra for $f = 0.0002$, 0.001, and 0.005. Although we do not know the actual f value for V1223 Sgr, we believe that the three values cover most of a possible range, and therefore.

In each spectrum, we fitted emission lines with Gaussians, and estimated their intensities accompanied with errors at the 90% confidence level as results listed in Table 3. From the fitting result, we calculated $R = z/(x+y)$, and plotted against f in Figure 11. Based on the calculated R results, we expect that we can clearly distinguish $f = 0.0002$ and 0.001 cases, but for 0.001 and 0.005 cases, discrimination may be possible only marginally within the errors.

Although plasma density diagnostics have been a very important method which can apply to broad range of densities and wavelengths, those with Fe XXV triplet lines are only possible with the SXS, and in particular, with targets that exhibits high-rate mass accretion. By observing V1223 Sgr, we would like to exploit the SXS capability and realize one of long-standing challenges anticipated for X-ray micro calorimeters.

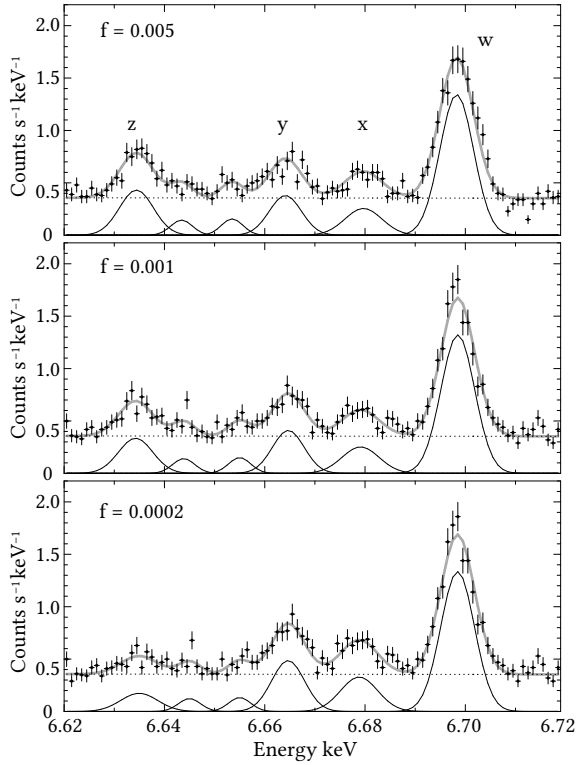


Figure 10: Fe XXV $K\alpha$ emission line spectra of the PSR of V1223 Sgr simulated assuming a 100-ks SXS observation. As used in Figure 8, we simulated three cases with different covering fractions $f = 0.005$, 0.001, and 0.0002.

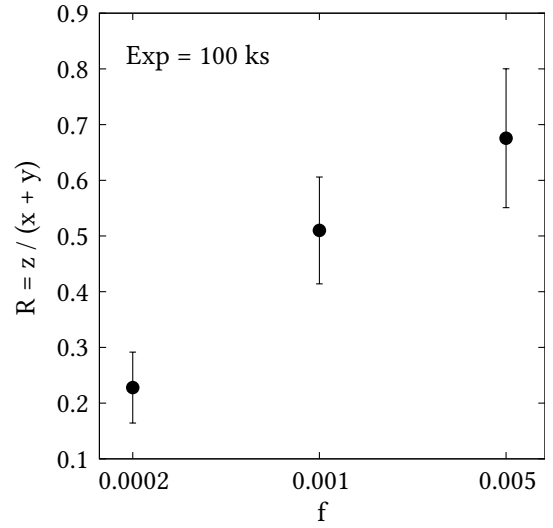


Figure 11: R ratios calculated from the x, y, and z intensities obtained from the gaussian fits of simulated 100-ks spectra. Associated errors are at the 90% confidence level.

4.4 Beyond Feasibility

The same observation of V1223 Sgr can be used to study reflection as a function of spin phase, and to search for gravitationally redshifted 6.4 keV line (see below). In addition, the spectrum of magnetic CVs are affected

Table 3: Results of the Gaussian fits to the simulated spectra of a 100-ks observation of V1223 Sgr.

f	Intensity (10^{-5} photons s^{-1} cm^{-2})				R
	w	x	y	z	
0.005	$4.80^{+0.25}_{-0.37}$	$1.00^{+0.18}_{-0.30}$	$1.29^{+0.11}_{-0.31}$	$1.54^{+0.22}_{-0.19}$	0.68 ± 0.12
0.001	$4.72^{+0.30}_{-0.37}$	$0.99^{+0.19}_{-0.27}$	$1.38^{+0.20}_{-0.19}$	$1.20^{+0.11}_{-0.21}$	0.51 ± 0.10
0.0002	$4.77^{+0.26}_{-0.33}$	$1.29^{+0.22}_{-0.18}$	$1.68^{+0.23}_{-0.18}$	$0.67^{+0.17}_{-0.18}$	0.23 ± 0.06

by complex partial covering absorber (Done & Magdziarz, 1998), including warm absorber features (Mukai et al., 2001). The SXS has large enough effective area and adequate spectral resolution below 1 keV to study these.

5 Reflection in accreting WDs

5.1 Background and Previous Studies

The primary X-rays emitted by accreting WDs can reflect off the WD surface and pre-shock accretion disk/column. This results in the reflection bump in >10 keV continuum and the 6.4 keV fluorescent line, and a physical understanding requires both to be fit in a self-consistent manner. An accurate characterization of the reflection bump is necessary for an accurate determination of the shock temperature, and hence the white dwarf mass. Unfortunately, most CVs and symbiotic stars are faint enough above 10 keV that the systematic uncertainties of the background in non-imaging detectors, including *Suzaku* HXD/PIN, have proved to be the limiting factor.

5.2 Prospects & Strategy

The combination of the high sensitivity of the *ASTRO-H* HXI for hard continuum and the spectral resolution of the SXS will allow us to measure the reflection fraction (both the hard continuum bump and the 6.4 keV fluorescent line) with an unprecedented accuracy. For the X-ray brightest magnetic CVs, this can be done in several spin phases, which will test angle-dependent models of reflection. The 6.4 keV line may exhibit Compton shoulder in some cases. As first reported by Hayashi et al. (2011) in V1223 Sgr, fluorescence from free-falling pre-shock gas will have detectable redshift due to its line-of-sight velocity of several $\times 1000$ km s^{-1} . A detection of redshifted Fe fluorescent line will improve our understanding of the accretion stream in magnetic CVs. This can lead to further improvements in the PSR model calculation and, consequently, spectral model calculations.

Hard X-ray continuum spectra of bright magnetic CVs may be observed with *NuSTAR* well before *ASTRO-H*, and the combination of the *NuSTAR* data with those of Fe $K\alpha$ lines from *XMM-Newton* or *Suzaku* may help to some extent. However, *ASTRO-H* data will definitely offer an improvement since they will allow a fully physical treatment of geometry, fluorescent line from WD surface and pre-shock gas and its Comptonization using simultaneous HXI and SXS data.

5.3 Targets & Feasibility

The same accreting magnetic CV, V1223 Sgr, as the PSR structure study is the most appropriate target because this is the brightest CV in the hard X-ray band (>10 keV), and therefore, we can expect sufficient photon counts within a realistic exposure. In addition, although this is a well studied classical magnetic CV, there are discrepancies among published analysis of the reflection component using instruments onboard past and current missions (e.g. Revnivtsev et al. 2004; Hayashi et al. 2011).

Figure 12 shows spin-resolved simulation spectra of V1223 Sgr. Spectral model of Yuasa (2013) has been convolved with the reflection model `reflect` assuming a large reflector that covers 50% of solid angle viewed

from the PSR. In this simulation, each spin-phase has net exposure of 20 ks (i.e. 100-ks observation is tentatively divided into five spin phases). Count rates in the HXI energy band are tabulated in Table 4.

Although differences between individual spin phases are not necessary obvious, the count rates can be used as a nice estimator of reflection fraction, and variation of them may constrain angular coverage of reflecting material (WD surface).

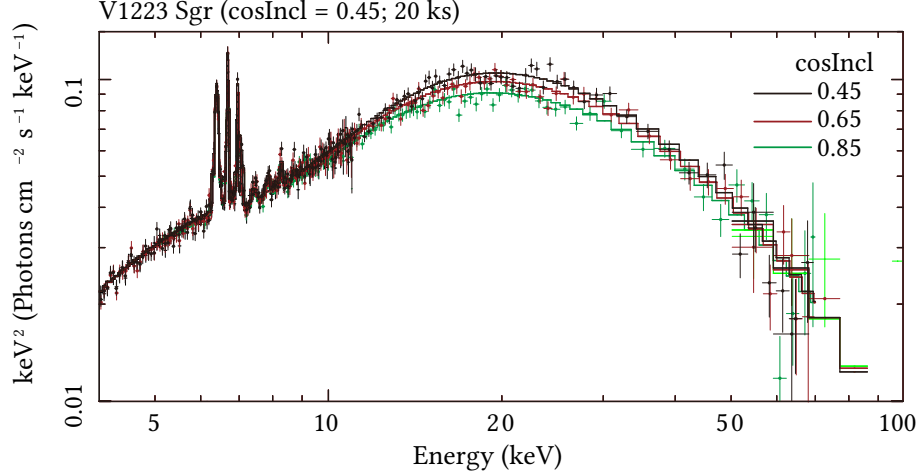


Figure 12: Faked SXI+HXI νF_ν spectra of V1223 Sgr. A total exposure of 100 ks is assumed. The presented spin-phase-resolved spectra are calculated with inclination angles (against the accretion column) $\cos \theta = 0.45, 0.65$, and 0.85 each with 20 ks (i.e. 100 ks exposure is divided into 5 spin phases).

Table 4: Simulated count rates of V1223 Sgr in the hard X-ray band.

$\cos \theta^1$	0.25	0.45	0.65	0.85
Count rate ²	1.334 ± 0.008	1.456 ± 0.009	1.550 ± 0.009	1.605 ± 0.009

¹ Inclination between the line of sight and the PSR vertical direction (i.e. normal vector of the WD surface where accreting gas lands).

² Total 10 – 70 keV count rate expected in the two HXI.

5.4 Beyond Feasibility

Based on previous studies, V1223 Sgr has a WD mass of $\sim 0.7 - 0.8 M_\odot$. Energies of fluorescent Fe $K\alpha$ line emitted at the WD surface should be affected by the gravitational redshift of an order or 1 eV. Although this gravitational redshift should be cross-checked by observing CVs with heavier WDs to overcome systematic uncertainty of SXS energy scale (see below), if we can measure redshift amount in V1223 Sgr, we will be able to improve reliability of our WD gravitational potential estimation, or mass estimation, supported by this which is independent from other measurable quantities such as shock temperature or free-fall velocity of pre-shock gas.

6 X-ray emission region in non-magnetic CVs

6.1 Background and Previous Studies

Observers have long assumed that the Keplerian accretion disk in non-magnetic CVs extend down to the white dwarf surface, and the boundary layer (BL) between the Keplerian disk and the white dwarf is the likely site of much of the X-rays we observe (Patterson & Raymond, 1985). The detailed structure of the boundary

layer, unfortunately, remains poorly understood. In high accretion rate cases, the boundary layer is expected to become optically thick, which should make it a soft X-ray source (say 20 eV blackbody), not a hard X-ray source. Yet, high accretion rate non-magnetic CVs are observed to emit hard X-rays. The origin of these hard X-rays, in systems that should have an optically thick boundary layer, is a major unanswered question. As proposed in Ishida et al. (2009), an accretion disk wind, which is a common feature of high accretion rate disks in CVs, may be connected with the hard X-ray emission in high accretion rates. At present, however, the study of wind in X-ray data is at a relatively early stage. Moreover, following the standard accretion disk Shakura & Sunyaev (1973), half of the gravitational energy is released in the accretion disk and, hence, the other half is released in BL. Observations in the extreme-ultraviolet band of SS Cyg and VW Hyi, however, revealed that the fractional energy radiated from BL is only $< 10\%$ of the disk luminosity (Mauche et al. 1991, 1995). According to classical theory, the temperature of BL in outburst is predicted to be $2\text{--}5 \times 10^5$ K (Pandel et al., 2005), whereas the temperature estimated by ultraviolet and optical emission lines is constrained to a significantly lower range of $5\text{--}10 \times 10^4$ K (Hoare & Drew, 1991). These discrepancies may be resolved if we assume that BL is terminated not on the static white dwarf surface, but on a rapidly rotating accretion belt on the equatorial surface of the white dwarf (Paczynski et al. 1978; Kippenhahn & Thomas 1978). Suggestions about the accretion belt, rotating at a speed close to the local Keplerian velocity, have been reported from a few non-magnetic CVs in outburst (Huang et al. 1996; Sion et al. 1996; Cheng et al. 1997; Szkody et al. 1998).

In addition, there is a question of whether the disk reaches the surface in the case of low accretion rate disks. Dwarf novae are large subclass of non-magnetic CVs in which the mass transfer rate from the secondary is low, the disk is cold and dim most of the time (quiescence) with occasional outbursts when the disk is hot and bright. This is generally interpreted in the framework of the disk instability model, or DIM (Lasota, 2001). However, an essential feature of DIM is that the accretion rate through a disk is highly dependent on the radial distance from the white dwarf: somewhat high near the outer edge, very low at the inner edge, hence matter accumulates in the disk throughout the quiescent interval. The basic version of the DIM therefore predicts an extremely low accretion rate onto the white dwarf during quiescence. The X-ray luminosity of quiescent dwarf novae immediately disproves this. One possible modification of DIM is that a central hole develops in quiescent dwarf nova.

6.2 Prospects & Strategy

A comparison of X-ray spectra of a dwarf nova in quiescence¹ and in outburst is highly instructive, and has been done with many X-ray satellites, most recently with *Suzaku* (Ishida et al., 2009). Figure 13 presents the XIS spectra taken during the quiescence and outburst states which have apparently distinctive Fe $K\alpha$ line profiles.

During quiescence, the fluorescent Fe $K\alpha$ line is composed of two components. The narrow component is interpreted as due to reflection off the WD surface and the broad component due to reflection off the inner disk. Given the equivalent widths of these component, the primary emission is from the BL and there is no room for a central hole in the disk. This important conclusion can be confirmed, and the quantitative results refined, with a relatively short *ASTRO-H* observation utilizing the high spectral resolution SXS.

In contrast, the fluorescent line is much broader during outburst. Ishida et al. (2009) inferred from this that the Fe $K\alpha$ lines and hard X-ray continuum are emitted from optically thin thermal plasma somewhere above the accretion disk (namely disk corona) as illustrated in Figure 14, and the Fe $K\alpha$ line profiles are double-peaked due to Doppler red and blue shifts caused by rapid rotation of the accretion disk and the corona. Moreover, if the system has moderate inclination and the plasma places close enough to the WD, a part of X-ray is occulted by the WD as figure 15 and the double-peaked lines are additionally distorted.

By precisely measuring the line profiles with the SXS, we will be able to determine the line-of-sight velocity of the disk corona and geometrical size of the corona (from equivalent width of fluorescence Fe $K\alpha$). The velocity can be related with Keplerian rotation speed, and thus, the location of the corona will be estimated enabling detailed study of disk corona which is not well understood in CVs.

¹Quiescent and outburst in this section refer to those in optical wavelength. In conventional X-ray wavelength, e.g. in $2\text{--}10$ keV, photon flux in quiescent state is higher than that of outburst state.

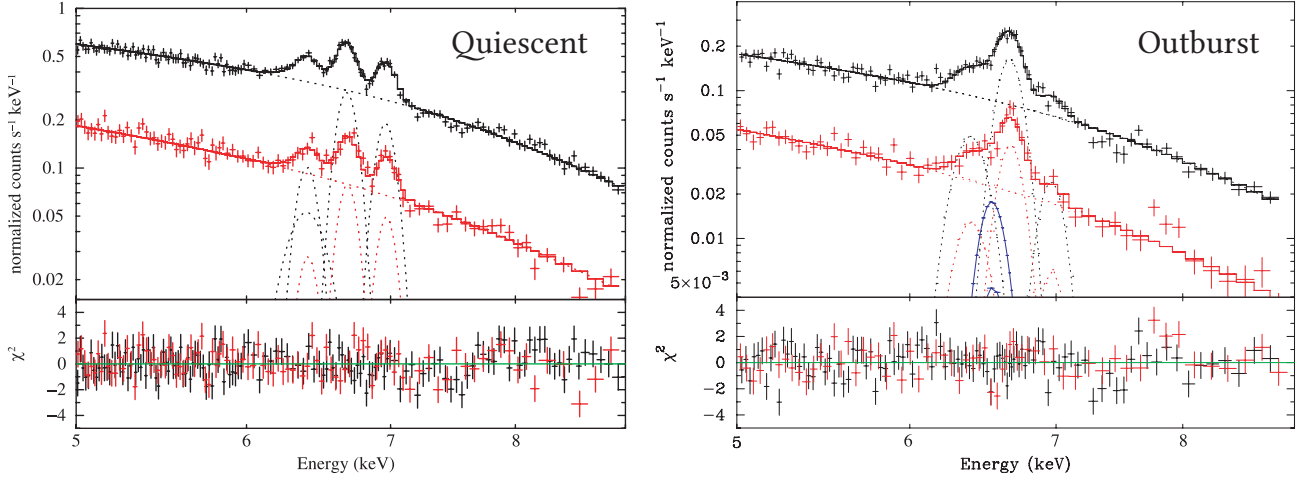


Figure 13: *Suzaku* XIS FI (black) and BI (red) spectra of SS Cyg in quiescence (left; 39 ks) and outburst (right; 56 ks). Note that the Fe $K\alpha$ line structures are apparently different in the two states. Adopted from Ishida et al. (2009).

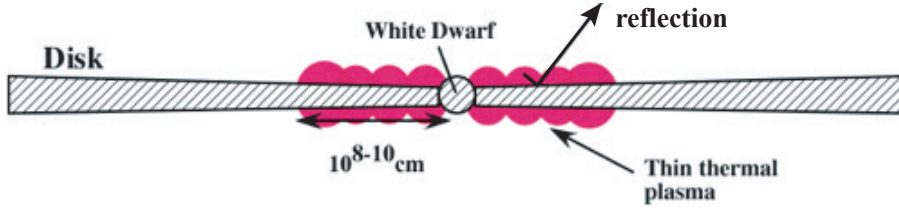


Figure 14: A schematic view of accretion disk and corona of SS Cyg in the outburst state. The pink bubble-like object labeled with “Thin thermal plasma” is thought to be the origin of hard X-ray continuum and the broadened Fe $K\alpha$ lines. Adopted from Ishida et al. (2009).

6.3 Targets & Feasibility

We believe that SS Cyg, which is the most widely studied dwarf novae, is the best target when studying disk corona and disk reflection with the SXS. Physical parameters of the system have been precisely measured as tabulated in Table 5, and therefore, we will be able to precisely correlate Doppler speed measured with the SXS to Keplerian motion estimating the innermost corona radius (and probably innermost disk radius). An outburst period of this system is about 50 days lasting ~ 10 days which is suitable for performing a time-constrained observation with *ASTRO-H*.

Table 5: System parameters of SS Cyg (Ishida et al. 2009 and references therein, with an updated distance from Miller-Jones et al. 2013).

Parameter	Value	Parameter	Value
M_{WD}	$1.19 \pm 0.02 M_{\odot}$	$M_{\text{secondary}}$	$0.704 \pm 0.002 M_{\odot}$
P_{orbital}	6.6 hr	P_{outburst}	~ 50 days
Inclination	$37^{\circ} \pm 5^{\circ}$	Distance	114 ± 2 pc

Figure 16 shows simulated Fe $K\alpha$ spectra of SS Cyg in outburst assuming 100 ks exposure and spectral model proposed in Ishida et al. (2009). Three separate innermost corona radii were assumed thus resulting different Doppler broadening of the lines. By fitting the simulated spectra with the model, we will be able to determine the disk inner radius within $\pm 5\%$ as well as plasma temperature of the corona based on the He-like and H-like line ratios. In this simulation, we used the SXS instrumental response files as follow:

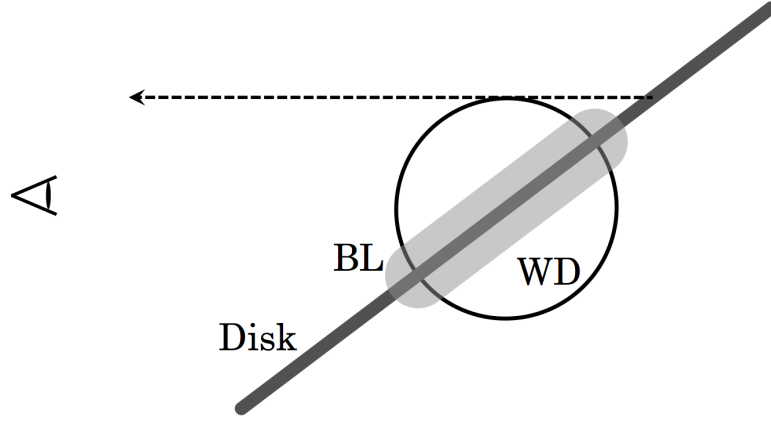


Figure 15: A schematic view of occultation of the accretion disk or BL by the WD.

- `ah_sxs_7ev_basefilt_20090216.rmf` (energy redistribution file),
- `sxt-s_120210_ts02um_intallpxl.arf` (auxiliary response file), and
- `sxs_cxb+nx_b_7ev_20110211_1Gs.pha` (background spectral file).

We also simulated spectra emitted by the plasma rotating with 1/10 of Kepler velocity at WD surface which is occulted by the WD with 100 ks exposure. The plasma distances from the WD were assumed to be the 0.1 times of the white dwarf radius. Figure 17 shows a comparison of fitting results of the simulated spectra with the occulted and non-occulted 1/10 Keplerian models. The larger residual is left with the non-occulted 1/10 Keplerian model. The no more than 7% accuracy for the distance between the plasma and the WD surface was obtained by fitting with the occulted 1/10 Keplerian model thawing the disk velocity. The significance of consideration of the occultation is $< 99.99\%$. Note that the uncertainties of instrument responses are not important for the spectral fitting to the distorted lines because the concerning energy ranges are narrow.

Thus, an SS Cyg observation will fully exploit the SXS capabilities, and constrain physical parameters of the disk corona which is not well studied in previous and on-going X-ray missions. Since hot disk corona is thought to be a common feature of accreting stellar black holes, development of understanding of disk corona in accreting non-magnetic CVs will infer ubiquity of disk corona in accretion physics independent of mass of accreting objects.

7 Anisotropic Radiative Transfer of Resonance photons

7.1 Background and Previous Studies

Resonance scattering by heavy ions can play important roles in radiative transfer, because the cross section of the resonance scattering is two orders of magnitude larger than that of Compton scattering in the X-ray band. In other words, resonance photons carry additional information regarding the physical conditions of the plasma. For example, optically thin hot plasmas in clusters of galaxies are optically thick for resonance scattering, but the resonance-scattering process is suppressed if a significant turbulent motion exists in the plasmas. Therefore, the equivalent widths of resonance lines can be used to quantify the amount of turbulence. The post-shock region (PSR) of magnetic CVs is another example in which resonant scattering can play a significant role. Typically, an optical depth of an accretion column in a magnetic CV for Compton scattering is of order $\tau_{CMP} \sim 10^{-1}$. However, the optical depth for resonance scattering process is of order $\tau_{RS} \sim 10^2$. Therefore, resonance photons carry (1) the information about the geometry of the column and/or (2) internal information of the plasma (velocity, temperature, and density gradients), through radiative transfer in the accretion column.

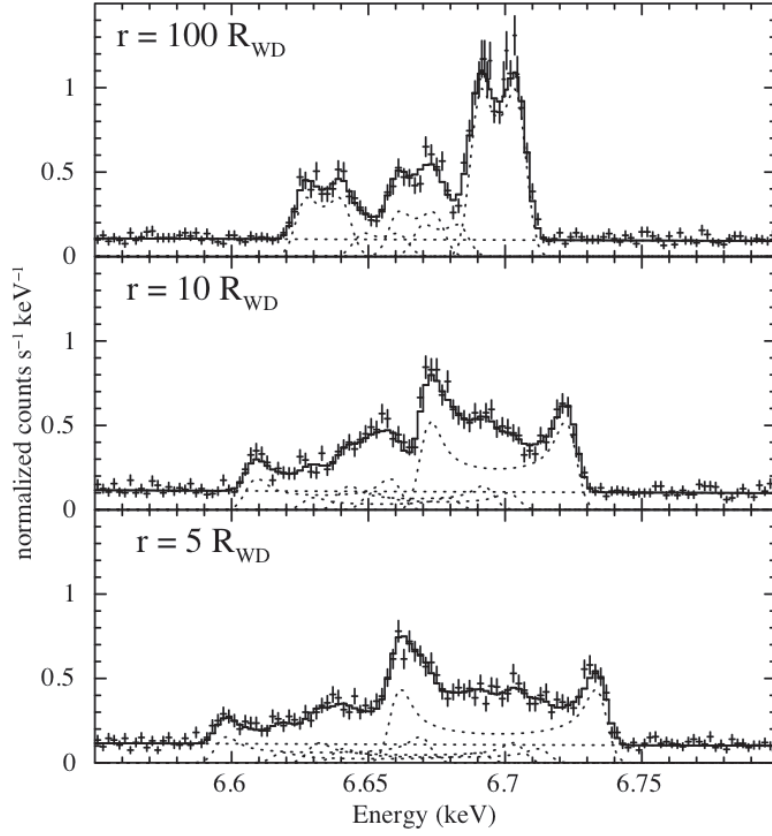


Figure 16: Simulated SXS spectra of SS Cyg. Assumed exposure is 100-ks each, and three spectra were calculated for disk inner radius r of $100 R_{\text{WD}}$, $10 R_{\text{WD}}$, and $10 R_{\text{WD}}$ from the top to the bottom.

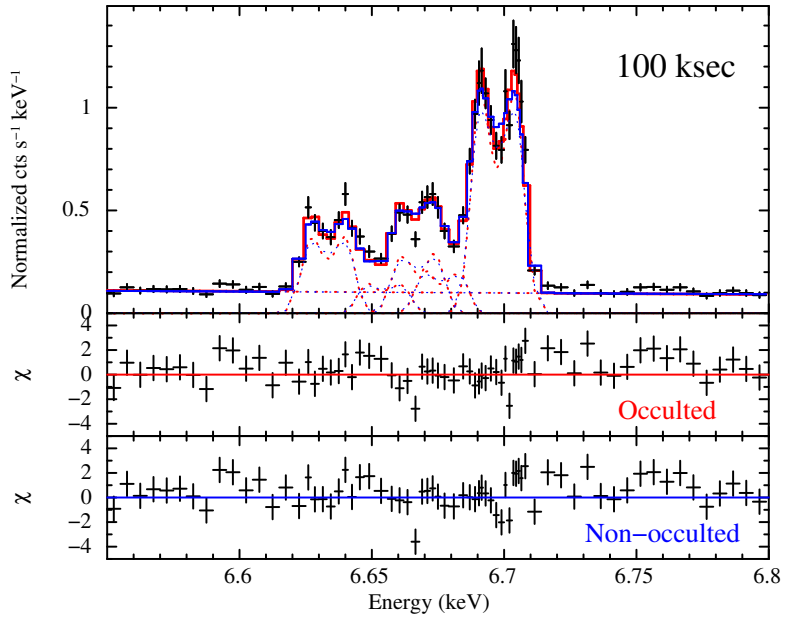


Figure 17: Top panel shows a simulated spectrum (black) for 100 ks exposure fitted with the occulted (red) and non-occulted (blue) 1/10 Keplerian models. The middle and the bottom panel show residuals for the two models.

Compared with plasmas in clusters of galaxies, one advantage of magnetic CV observations is that we can scan

various viewing angles to the plasma using the spin of the WD.

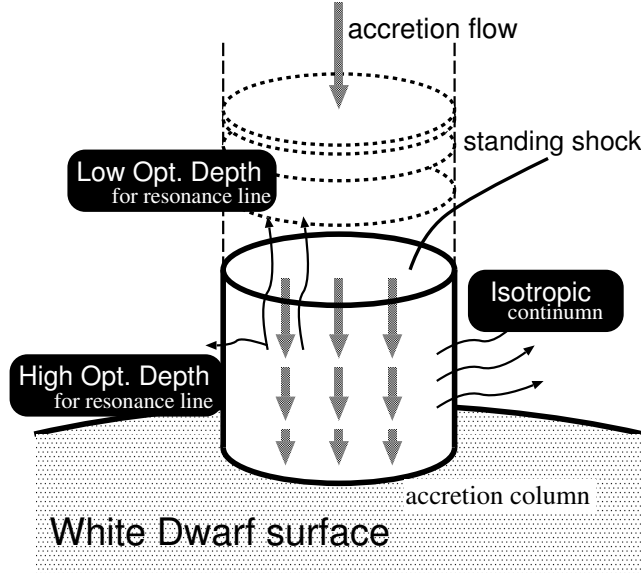


Figure 18: Schematic view of the accretion column of magnetic CVs and their optical depths to Compton and resonance scatterings. Adopted from Terada et al. (2001).

The idea of anisotropic radiative transfer of resonance photons in the accretion columns of polar type magnetic CVs was originally proposed briefly in Terada et al. (1999). Only the surface of the accretion column is observed by resonance lines due to the high opacity, whereas thermal photons show isotropic emission (i.e., whole volume is seen). Therefore, the equivalent width of resonance line will be enhanced when we observe the accretion column from the pole-on direction when it has flat coin-like shape. In addition to such geometrical effects, another collimation effect due to velocity gradient in the column is also expected Terada et al. (2001). As shown in the schematic view of the accretion column in Figure 18, the velocity of the bulk flow of the gas has a vertical gradient, and thus the resonance scattering optical depth τ_{RS} is reduced in the vertical direction, while it remains optically thick in the horizontal direction. Therefore, the resonance photons preferentially escape in the vertical direction of the column. Note that the anisotropy in σ_{RS} can be suppressed by the thermal broadening effect on σ_{RS} ; the vertical structure of the temperature should be considered in the radiative transfer. These effects are numerically clarified using Monte Carlo simulations of the radiative transfer in the accretion column (Terada et al., 2001).

Observationally, anisotropic transfer of resonance photons was marginally confirmed by phase-resolved analyses of Fe K lines with ASCA observation of the polar, V834 Cen (Terada et al., 2001) and tested for other 18 magnetic CVs observed with ASCA (Terada et al., 2004). These observations indicate that this effect is significant in polars, but not in intermediate polars. The likely explanation for the difference between the two subclasses of magnetic CVs is the geometry. Intermediate polars, accretion is via a partial disk, in the form of “accretion curtains” that cover large ranges in magnetic latitude, and photons can easily escape preferentially perpendicular to the curtains.

However, it is important to note that the relatively poor energy resolution of the ASCA SIS limited our ability to separate pure resonance lines from the blend of Fe K lines; the Fe XXVI K_{α} line is the pure resonance line but is weak and is difficult to be separated from Fe XXV K_{α} and/or fluorescent Fe lines. Needless to say, it is impossible to distinguish resonance (6.698 keV), inter-combination (6.673 keV), and forbidden (6.637 keV) lines of Fe XXV K_{α} blends with CCD. As for lighter elements (O, Mg, Si, S, etc), the anisotropy effect by the bulk velocity gradient is expected to be strongly suppressed by the thermal Doppler broadening, and thus the effect could not be tested by grating observations with *Chandra* or *XMM-Newton*. Therefore, only *ASTRO-H* SXS observations can test the anisotropic radiative transfer of resonance photons.

7.2 Prospects & Strategy

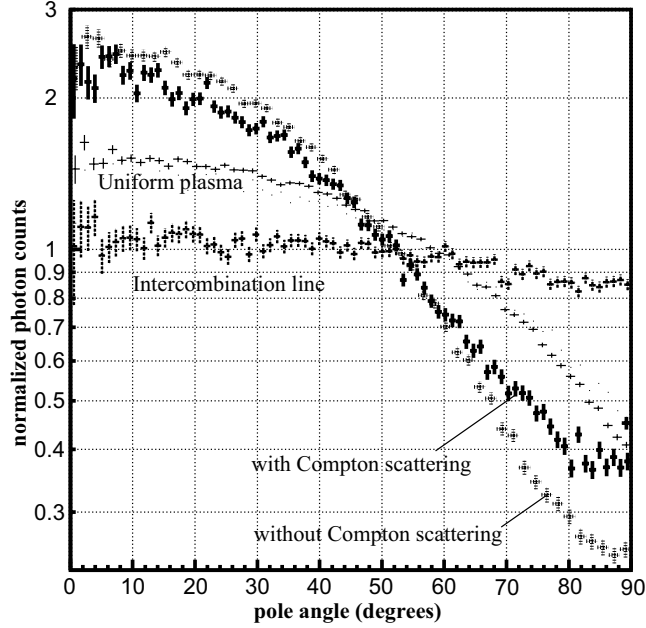


Figure 19: Angular distributions of resonance and inter-combination lines of Fe XXV K_α . Adopted from Terada et al. (2001).

According to the Monte Carlo simulation of radiative transfers of resonance and continuum photons in the accretion column by Terada et al. (2001), we can expect a factor of 2 or 3 enhancement at maximum. Figure 19 shows a distribution of photons as a function of the angle from the vertical axis of the column (pole angle; 0 and 90 degrees mean pole-on and side-on views). For inter-combination lines, which must show isotropic emission, the photon flux has almost no dependency on the pole angle, as expected. On the other hand, resonance photons is enhanced to the pole-on direction by factor 2 or 3, as illustrated in the vertical axis of the figure. For reference, the figure shows plots without Compton scattering or without vertical gradient of the bulk velocity.

By precise measurements of enhancement of resonance photons with the SXS, we can test the assumption in the simulation on the structure of the plasma (i.e., the vertical gradient of the bulk velocity, temperature, and densities) independently from the measurements of the continuum or other lines described in the previous sections.

7.3 Targets & Feasibility

Figure 20 shows simulated phase-resolved X-ray spectra around Fe K band by the Monte Carlo simulation (Terada et al., 2001), under the assumption that we can observe the pole angle from 0 to 90 degrees. Thus, we can expect the enhancement on the resonance line, as a function of Doppler shift by the vertical bulk motion of the gas. This is the direct verification of the anisotropic resonance-scattering effect.

We must select a target that allows us to observe a wide range of pole angles, using the tabulated values of magnetic colatitude β and the inclination angle i . They are summarized in Table 4 of Terada et al. (2001); by this criterion, the best candidates are VY For and EK UMa; AM Her, V834 Cen, and GG Leo (=RX J1015+09), are also good candidates. Once we also considering the known hard X-ray fluxes, the latter three are more suitable targets, however. In addition, polars are known to have low states in which the X-ray flux can drop by an order of magnitude or more. An observation during a low state will likely be photon-starved and will not allow us to take advantage of the spectral resolution of the *ASTRO-H* SXS.

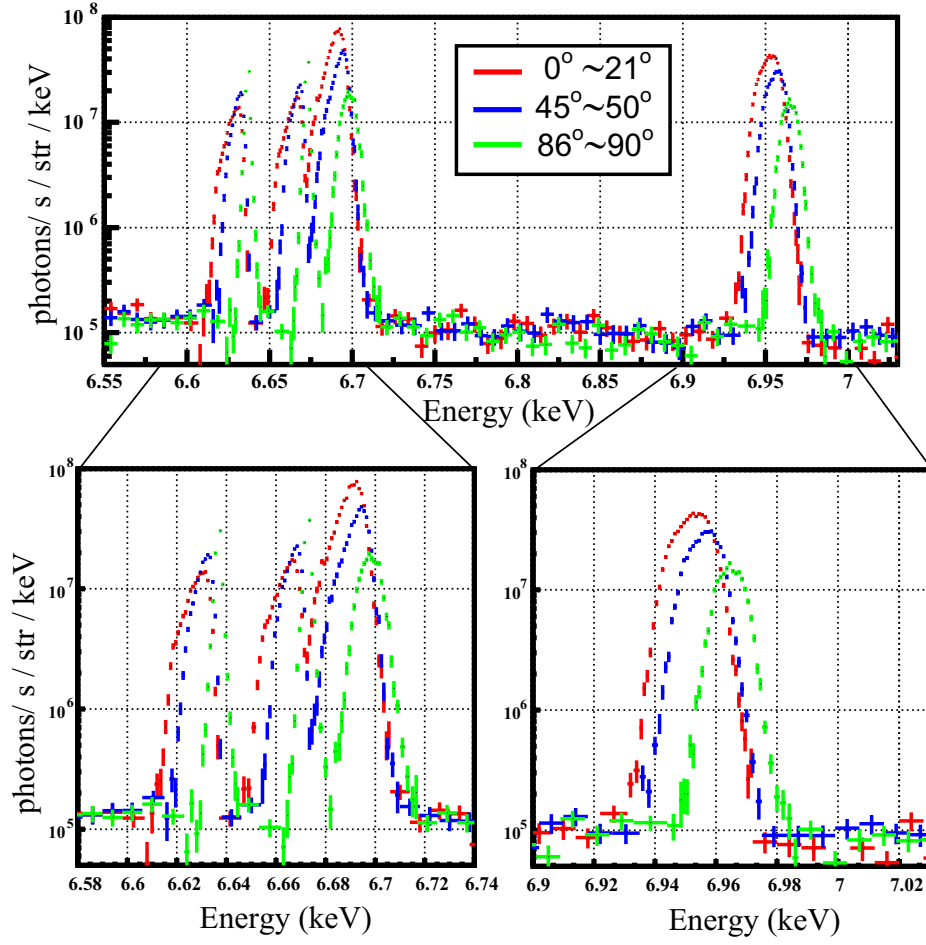


Figure 20: Phase resolved energy spectra for iron K_α lines calculated by the Monte Carlo simulation (Terada et al., 2001). Adopted from Terada (2002).

References

- Aizu, K. 1973, *Prog. Theor. Phys* 49, 1184
- Cheng, F. H., Sion, E. M., Horne, K., Hubeny, I., Huang, M., & Vrtilik, S. D. 1997, *AJ*, 114, 1165
- Done, C. & Magdziarz, P. 1998, *MNRAS*, 298, 737
- Gabriel, A. H. & Jordan, C. 1969, *MNRAS*, 145, 241
- Hayashi, T., Ishida, M., Terada, Y., Bamba, A., & Shionome, T. 2011, *PASJ*, 63, 739
- Hellier, C. 1997, *MNRAS*, 291, 71
- Hoare, M. G., & Drew, J. E. 1991, *MNRAS*, 249, 452
- Huang, M., Sion, E. M., Hubeny, I., Cheng, F. H., & Szkody, P. 1996, *ApJ*, 458, 355
- Ishida, M., Okada, S., Hayashi, T., Nakamura, R., Terada, Y., Mukai, K., & Hamaguchi, K. 2009, *PASJ*, 61, S77
- Kaastra, J. S., Mewe, R. & Nieuwenhuijzen, H. 1996, 11th Colloquium on UV and X-ray Spectroscopy of Astrophysical and Laboratory Plasmas, 411
- Kennea, J.A., Mukai, K., Sokoloski, J.L., Luna, G.J.M., Tueller, J., Markwardt, C.B., & Burrows, D.N. 2009, *ApJ*, 701, 1992
- Kippenhahn, R., & Thomas, H.-C. 1978, *A&A*, 63, 265
- Lasota, J.-P. 2001, *New Astron. Rev.* 45, 449
- Mauche, C. W., Wade, R. A., Polidan, R. S., van der Woerd, H., & Mauche, C. W., Raymond, J. C., & Mattei, J. A. 1995, *ApJ*, 446, 842
- Paerels, F. B. S. 1991, *ApJ*, 372, 659
- Mauche, C.W., Liedahl, D.A., & Fournier, K.B. 2003, *ApJ*, 588, L101
- Miller-Jones, J.C.A., Sivakoff, G.R., Knigge, C., Kording, E.G., Templeton, M., & Waagen, E.O. 2013, *Science*, 340, 950
- Mukai, K., Kallman, T., Schlegel, E., Bruch, A., Handler, G., & Kemp, J. *ASPC*, 251, 90
- Nauenberg, M., 1972, *ApJ*, 175, 417
- Palmeri, P., Mendoza, C., Kallman, T.R., Bautista, M.A. & Melendez, M. 2003, *A&A*, 410, 359
- Pandel, D., Córdova, F. A., Mason, K. O., & Priedhorsky, W. C. 2005, *ApJ*, 626, 396
- Patterson, J. & Raymond, J.C. 1985, *ApJ*, 292, 535
- Paczyński, B. 1978, in *Nonstationary Evolution of Close Binaries*, ed. A. Zytkov (Warsaw: Polish Academy of Science), 89
- Porquet, D., Dubau, J., & Grosso, N., 2010, *SSR*, 157, 103
- Revnivtsev, M., Lutovinov, A., Suleimanov, V., Sunyaev, R., & Zheleznyakov, V. 2004, *A&A*, 426, 253
- Reis, R.C., Wheatley, P.J., Gänsicke, B.T., & Osborne, J.P. 2013, *MNRAS*, 430, 1994
- Sion, E. M., Cheng, F.-H., Huang, M., Hubeny, I., & Szkody, P. 1996, *ApJ*, 471, L41
- Shakura, N. I., & Sunyaev, R. A. 1973, *A&A*, 24, 337
- Suleimanov, V., Revnivtsev, M. & Ritter, H. 2005, *A&A*, 435, 191
- Szkody, P., Hoard, D. W., Sion, E. M., Howell, S. B., Cheng, F. H., & Sparks, W. M. 1998, *ApJ*, 497, 928
- Terada, Y., Kaneda, H., Makishima, K., Ishida, M., Matsuzaki, K., Nagase, F., & Kotani, T. 1999 *PASJ* 51, 39
- Terada, Y., Ishida, M., Makishima, K., Imanari, T., Fujimoto, R., Matsuzaki, K., & Kaneda, H. 2001, *MNRAS*, 328, 112
- Terada, Y. 2002, Ph.D Thesis, University of Tokyo
- Terada, Y., Ishida, M., & Makishima, K. 2004, *PASJ*, 56, 533
- Werner, K., Rauch, T., Kruk, J.W. & Kurucz, R.L. 2011, *A&A*, 531, A146
- Yuasa, T., Nakazawa, K., Makishima, K., Saitou, K., Ishida, M., Ebisawa, K., Mori, H., & Yamada, S. 2010, *A&A*, 520, A25
- Yuasa, T. 2013, *Springer Theses*, ISBN13: 978-4431542186